PUCRS

ESCOLA POLITÉCNICA
PROGRAMA DE PÓS-GRADUAÇÃO EM CIÊNCIA DA COMPUTAÇÃO
MESTRADO EM CIÊNCIA DA COMPUTAÇÃO

KATHERINE BIANCHINI ESPER

NEURO-SYMBOLIC AUTOMATED DESIGN OF FMRI PARADIGMS

Porto Alegre
2022

PÓS-GRADUAÇÃO - *STRICTO SENSU*

Pontifícia Universidade Católica
do Rio Grande do Sul

PONTIFICAL CATHOLIC UNIVERSITY OF RIO GRANDE DO SUL
SCHOOL OF TECHNOLOGY
COMPUTER SCIENCE GRADUATE PROGRAM

NEURO-SYMBOLIC AUTOMATED DESIGN OF FMRI PARADIGMS

KATHERINE BIANCHINI ESPER

Master Thesis submitted to the Pontifical Catholic University of Rio Grande do Sul in partial fulfillment of the requirements for the degree of Master in Computer Science.

Advisor: Prof. Dr. Felipe Meneguzzi

Porto Alegre
2022

Ficha Catalográfica

E77n Esper, Katherine Bianchini

Neuro-symbolic automated design of fMRI paradigms / Katherine Bianchini Esper. – 2022.
60p.
Dissertação (Mestrado) – Programa de Pós-Graduação em Ciência da Computação, PUCRS.

Orientador: Prof. Dr. Felipe Meneguzzi.

1. Artificial Intelligence. 2. Neuroimaging. 3. fMRI. 4. Automated Planning. I. Meneguzzi, Felipe. II. Título.

Elaborada pelo Sistema de Geração Automática de Ficha Catalográfica da PUCRS
com os dados fornecidos pelo(a) autor(a).
Bibliotecária responsável: Clarissa Jesinska Selbach CRB-10/2051

KATHERINE BIANCHINI ESPER

NEURO-SYMBOLIC AUTOMATED DESIGN OF FMRI PARADIGMS

This Master Thesis has been submitted in partial fulfillment of the requirements for the degree of Master in Computer Science, of the Computer Science Graduate Program, School of Technology of the Pontifical Catholic University of Rio Grande do Sul

Sanctioned on August 29, 2022.

COMMITTEE MEMBERS:

Prof[a]. Dr[a]. Isabel Harb Manssour (PPGCC/PUCRS)

Prof. Dr. André Grahl Pereira (PPGC/UFRGS)

Prof. Dr. Felipe Meneguzzi (PPGCC/PUCRS - Advisor)

DESIGN AUTOMATIZADO NEURO-SIMBÓLICO DE PARADIGMAS DE RMF

RESUMO

As técnicas de neuroimagem têm sido amplamente utilizadas nas últimas décadas para avaliar os padrões de ativação do cérebro. O projeto de tarefas é um dos desafios mais importantes para os estudos de neuroimagem, para que seja possível obter a melhor modelagem para avaliar os padrões cerebrais de um sujeito e entre os sujeitos. Os experimentos de Ressonância Magnética funcional (RMf) dependem de um design de paradigmas preciso e eficaz, selecionando as melhores sequências de estímulos para ativar regiões cerebrais específicas. Neste projeto, propomos o uso de *Planning Domain Definition Language* (PDDL+) para modelar diferentes paradigmas e suas respectivas ativações cerebrais, resultando em uma ferramenta para geração automática de estímulos para exames de RMf. Desenvolvemos uma aplicação de planejamento automatizado para pesquisa neurocientífica e planejamento pré-cirúrgico. O primeiro deve ajudar a garantir um desenho experimental que permita a análise das regiões cerebrais de interesse do estudo. O último, deve ajudar os cirurgiões a selecionar os estímulos corretos para uma exploração pré-cirúrgica não invasiva das funções cognitivas que podem ser afetadas pelo desbridamento de lesões cerebrais.

Palavras-Chave: inteligência artificial, neuroimagem, RMf, planejamento automatizado.

NEURO-SYMBOLIC AUTOMATED DESIGN OF FMRI PARADIGMS

ABSTRACT

Neuroimaging techniques have been widely used in recent decades to assess brain activation patterns for neuroscience. Task design is the most important challenge for neuroimaging studies to achieve the best modeling for assessing brain patterns within and across subjects. Specifically, functional magnetic resonance imaging (fMRI) experiments rely on the precise and effective paradigm design, selecting the best sequences of stimuli to activate specific brain regions. In this project, we propose to use *Planning Domain Definition Language* (PDDL+) to model fMRI paradigms so that neuroscientists can design neuroimaging paradigms in a declarative way. We develop an application of automated planning for neuroscience research and presurgical planning, resulting in and a tool for automatic stimuli generation for fMRI scans. The former should help to ensure an experimental design that allows the analysis of the brain regions that are interesting in the study. The latter should help surgeons select the correct stimuli for a presurgical non-invasive exploration of the cognitive functions that might be affected by debridement of brain lesions.

Keywords: artificial intelligence, neuroimaging, fMRI, automated planning.

LIST OF FIGURES

LIST OF TABLES

CONTENTS

1. INTRODUCTION

Functional Magnetic Resonance Imaging (fMRI) is a non-invasive technique widely used to analyze brain function [17]. This imaging technique measures neuronal activity by detecting concentration changes of oxy- and deoxy-hemoglobin in the stimulated area [38]. This is an indirect measure called Blood Oxygen Level Dependent (BOLD) or hemodynamic response [36, 30]. To develop an fMRI study, a researcher starts with a research question concerning either brain function or an anatomical region of interest. Using the research question as guidance, researchers design an fMRI protocol, which includes various imaging parameters, but importantly for this work, it also includes an fMRI paradigm. Paradigms are the activities performed or stimuli received by the subject during a study [3] to evoke a hemodynamic response or brain activation in certain brain areas. Common paradigms include visual, motor, language, and memory, each of which include a series of possible tasks or stimuli designed to activate the respective brain regions. To activate the brain area of interest, researchers select a paradigm expected to increase the BOLD signal of those regions [30].

Since there are extensive study designs and software available for fMRI projects, researchers often build new fMRI protocols by choosing available paradigm designs that they can combine in a way that helps them answer their research question [3, 25]. Alternatively, researchers design new paradigms when they fail to find a suitable existing one. In both cases, the researcher's task consists of conducting a literature review of studies related to their research question and then picking existing paradigms or choosing ones that could be adapted in creating a new one. Ultimately, a successful fMRI experiment relies on precise and effective paradigm design, while at the same time aim to minimize its overall cost of each scan, since the cost of an fMRI scan is directly proportional to the time it takes, due to the substantial power requirements of maintaining an fMRI scanner's superconducting magnets.

Besides its applicability to neuroscientific research, the clinical use of fMRI is becoming a standard tool in presurgical planning [27, 6]. The surgical treatment of brain tumors seeks to complete removal of the abnormality, while minimizing the risk of inducing neurological deficits. The Intracarotid Amobarbital Test (IAT or Wada test) is universally relied upon as a prognostic test for patients with intractable temporal lobe epilepsy who are candidates for neurosurgical intervention. As fMRI is a repeatable procedure and Wada is a very invasive test, it would be advantageous to create validated paradigms to allow fMRI use instead of the Wada test.

The more or less *ad hoc* way in which researchers design new paradigms points to the need for a principled, ideally automated, method to design paradigms from scratch, given specific requirements from either a neuroscientist or surgeon. Thus, our main goal is to develop an application of automated planning for both neuroscience research and

presurgical planning, resulting in a tool for automatic stimuli generation for fMRI scans. We propose to solve the dual problem of effective paradigm design and scan cost minimization using PDDL+ to automatically generate fMRI paradigms. In this project, we combine automated planning and neuroimage techniques to automatically derive planning domains that represent the relation of stimuli in fMRI with various cerebral regions of interest (1); numerically describe the brain activation, based on the BOLD signal (2); test the paradigm planner in real cases to see the effectiveness of the paradigms created (3). In this research, we design planning domains for the most common neurological functions localized in presurgical planning: language dominance and lateralization, motor and memory skills [42, 49, 28].

This work is divided into six chapters. Chapter 2 briefly provides background of the issues relevant to the development of the project. Initially, the concepts related to Magnetic Resonance Imaging and design of fMRI studies are presented, followed by the presurgical planning using fMRI. The Chapter 3 summarizes the formalisms for Automated Planning and Temporal Numeric Planning. In Chapter 4 we detail the methods used to model fMRI studies in PDDL+. Finally, Chapter 5 presents the experiments performed and the results of this research. We also discuss related work in Chapter 6 and, the conclusions in Chapter 7.

2. NEUROIMAGE BACKGROUND

In this chapter, we briefly review key required background to our contributions. Section 2.1 provides an introduction to Magnetic Resonance Imaging (MRI) and Section 2.2 to functional MRI and the Blood Oxygen Level-Dependent (BOLD) signal. Section 2.3 describes what fMRI paradigms are and how they are designed. Finishing the background on neuroimaging, the Section 2.4 briefly introduces presurgical planning using fMRI, which is the focus of our research.

2.1 Nuclear Magnetic Resonance Imaging

Nuclear Magnetic Resonance Imaging, or just Magnetic Resonance Imaging (MRI), is one of the most well-known medical modalities for obtaining anatomical information on a specific area of interest. It is a method of diagnostic imaging with wide clinical application and in growing development in the scientific area, as it is possible to obtain high-resolution images capable of identifying abnormalities in tissues and various structures of the human body. MRI is a neuroimaging method in which the magnetic properties of different brain tissues can be measured, being possible to observe changes in the behavior of substances and brain regions. The image is the result of the interaction of the strong magnetic field produced by the equipment with the hydrogen protons of the tissues [24].

The hydrogen atom is the most abundant in the human body and the simplest in the periodic table [24]. Its nucleus has a proton, which is a positively charged particle. Because the proton moves around its own axis, it has angular momentum (or spin) and a magnetic momentum. This spin movement generates its magnetic field around it, behaving like a small magnetic dipole or a magnet. The protons in the human body are constantly under the action of the Earth's magnetic field, which is a very weak field. Due to this field, the magnetic moments have a random spatial orientation that generates a resulting magnetization in each tissue voxel equal to zero. A voxel is a volumetric element corresponding to the pixel of an image, but in three dimensions, being used for spatial location. When the body's hydrogen protons are placed under the action of an external and stronger $B0$ magnetic field, they orient themselves according to the direction of the applied field, pointing in parallel or antiparallel to it. This orientation indicates the two energy levels that the proton may be in, the magnetization vector of each voxel being the result of the vector sum of all spins.

The magnetic momentum of a proton can be represented through the coordinate axis (x, y, and z), the z-axis being called longitudinal and the transverse is the plane formed by x and y. The values that indicate the relaxation process, which is the time that the vector resulting from magnetization takes to return to its equilibrium state after

the application of the magnetic field, are called T_1 and T_2. The constant T_1 is related to the magnetization return time for the longitudinal axis and T_2 to the magnetization decay in the transverse plane. Figure 2.1 shows the relaxation times to fat and water in the transverse and longitudinal planes. The time required for magnetization in the longitudinal plane to reach 63 percent of the initial value is called T_1 (Figure 2.1a) and for the transverse plane to reach 37 percent of its initial value, T_2 (Figure 2.1b).

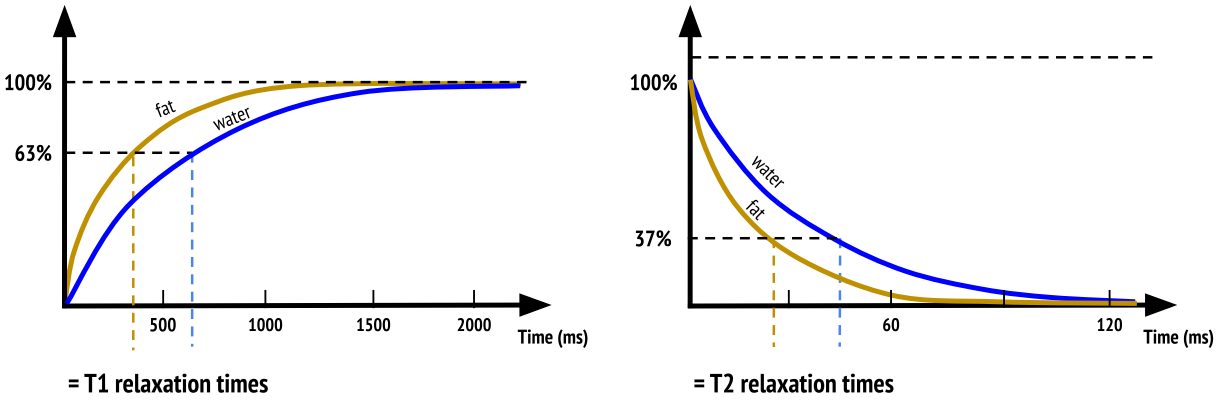

(a) Longitudinal magnetization (b) Transverse magnetization

Figure 2.1: T_1 and T_2 relaxation times to fat and water

One of the advantages of using MRI over other imaging methods is the differentiation of tissues through the relaxation time of T_1 and T_2 constants. These differences in values for each tissue allow contrast to be generated between the structures, which may result in different types of images. Figure 2.2 shows the difference between images weighted by T_1 (Figure 2.2a) or T_2 (Figure 2.2b) sequences. Each of these types can have a different application, the T_1-weighted image being better for looking at the white and gray brain structures and substances, while the T_2-weighted image is better for identifying lesions in the white matter.

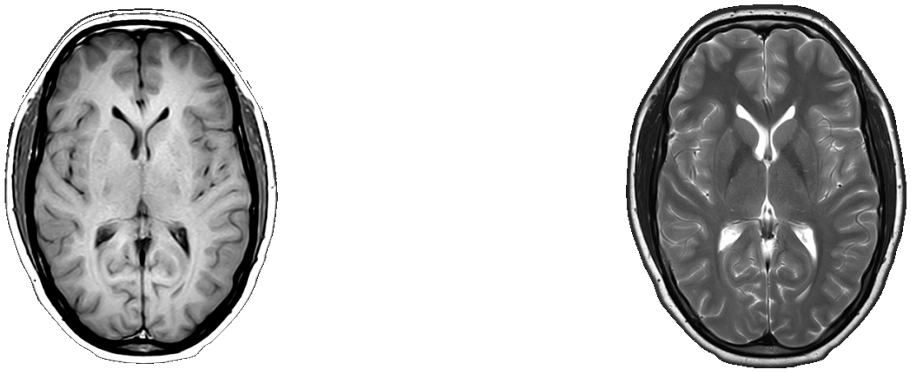

(a) T_1-weighted image (b) T_2-weighted image

Figure 2.2: MRI sequences examples: T_1- (a) and T_2-weighted (b) images

2.2 Functional Magnetic Resonance Imaging

Functional Magnetic Resonance Imaging (fMRI) is a noninvasive imaging technique for obtaining three-dimensional images demonstrating time-varying changes in brain metabolism [24, 10]. It is an established and widely used technique for mapping brain function from the measurement of neuronal activity by local oxygenation of blood. The signal variation is described by the Blood Oxygenation Level-Dependent or BOLD signal. fMRI detects the BOLD signal as an indicator of neuronal activity associated with the performance of a specific *task* [10, 16]. An example of how to explore motor functions in the brain using BOLD signal is presented in the Figure 2.3.

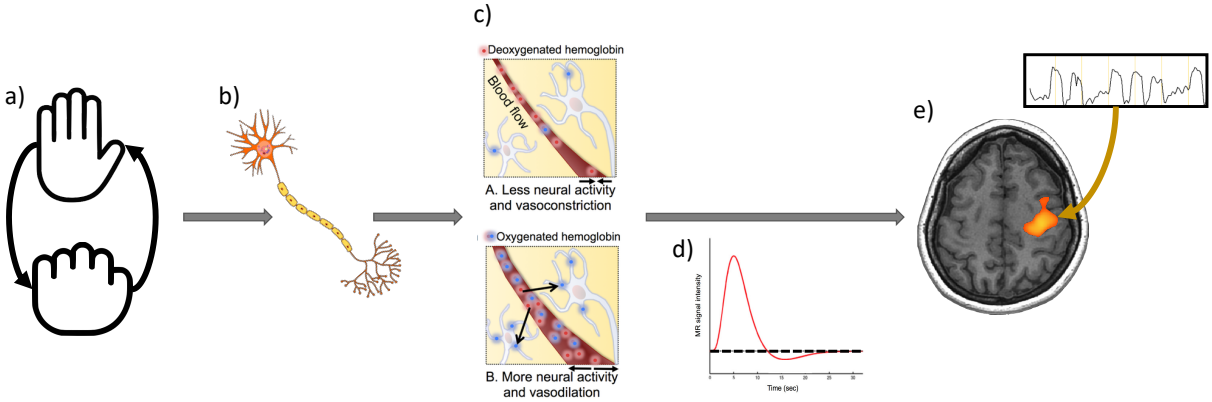

Figure 2.3: Blood Oxygenation Level Dependent signal

If the patient is asked to move their right or left hand during the exam (Figure 2.3a), there will be an excitatory neuronal activity in the related motor areas (Figure 2.3b). This will increase the consumption of oxygenated blood in the motor cortex, dilating the blood vessels (Figure 2.3c) and increasing the signal intensity in the motor area (Figure 2.3d). The fMRI BOLD response can be seen after some steps of data processing. This data processing (or preprocessing) allows the investigator to see which brain areas are associated with the presented stimuli (Figure 2.3e). The fMRI BOLD response has a characteristic curve composed of seven phases. Figure 2.4 illustrates the seven phases of the BOLD signal [24] with the corresponding sequential numeric values.

The BOLD signal is evaluated according to the concentrations of oxygenated hemoglobin (*oxyhemoglobin*) and deoxygenated hemoglobin (*deoxyhemoglobin*). During

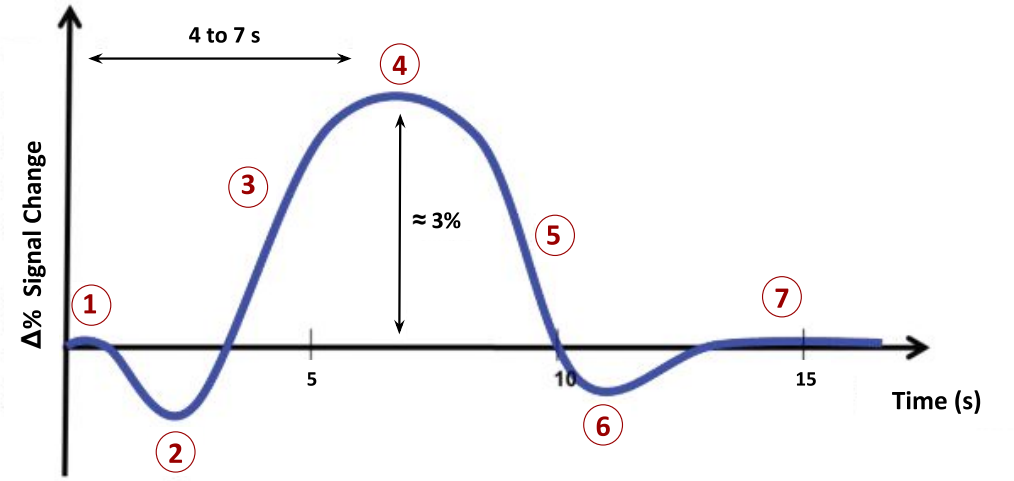

Figure 2.4: BOLD signal phases: baseline (1), initial drop (2), increased BOLD signal (3), peak of the BOLD signal (4), BOLD signal reduction (5), posterior fall (6), and return to baseline (7) [24]

neuronal activation, an increase in the concentration of the deoxyhemoglobin, may occur, causing the initial drop in the curve (phase 2). In sequence, the increase in the oxy- and deoxy-hemoglobin ratio leads to the peak of the BOLD signal (phases 3 and 4), which remains at the peak as long as the stimulus is maintained. At the end of the stimulus, the signal may show a further drop (phase 6) to finally return to the baseline (phase 7). Part of data preprocessing consists of searching for this curve model in the brain activation timeline, as illustrated in Figure 2.3e.

As a tool for studying brain functions, fMRI is used by different researchers and professionals, for example, psychologists, psychiatrists, neurologists and neuroscientists [51]. fMRI has clinical and research applications, and both can provide an understanding of brain pathologies. Research applications are the most common uses, because fMRI allows the study of learning disabilities [7], and the effects of drug dependency [26], for example. Also can be useful to reveal the neural underpinnings of autism [23, 21] and various cognition and clinical abnormalities in brain function..

fMRI use the time-varying changes to explore cerebral functions, like memory abilities, language comprehension, and motor skills. To be able to evoke each brain function, it is necessary to correctly choose the type of stimulus that the research participant, for example, will receive. Choosing these stimuli is one of the most important steps in the design of fMRI studies.

2.3 Design of fMRI studies

During an fMRI task, there is an increase in neuronal activity in the brain area associated with some stimulus [3, 25]. For example, during a motor skill stimulus, there is

neuronal activation in the motor area. *Paradigms* are the activities performed or stimulus received by the subject during a study to evoke a hemodynamic response or brain activation in certain brain areas [3]. It represents the set of cognitive stimuli that the individual must perform at the time of the exam. Common paradigms include visual, motor, language, and memory, each of which include a series of possible tasks designed to activate the respective brain regions. To activate the brain area of interest, researchers select a paradigm expected to increase the BOLD signal of those regions [30]. Since there are extensive study designs and software available for fMRI projects, researchers often build new fMRI protocols by choosing available paradigm designs that they can combine in a way that helps them answer their research question [3, 25]. Alternatively, researchers design new paradigms when they fail to find an existing one. In both cases, the researcher's task consists of conducting a literature review of studies related to their research question and then picking existing paradigms or choosing ones that could be adapted in creating a new one.

There are two categories to stimulus presentation possibilities: block- and event-related. These are the most established and efficient approaches for the paradigm design [25] and differ in relation to the time that each stimulus is presented on the screen. The Figure 2.5 shows an example of how stimuli are presented for block- and event-related designs. In the first approach, each block is presented for relatively long periods where the cognitive state is maintained. Event-related designs are composed of discrete events, where the stimuli are presented for shorter periods and used to the decomposition of cognitive states [29]. These two possibilities to stimulus presentation allow analyzing the differences in the temporal characteristics between the rapid motion-induced and the slower BOLD signal changes. In both cases, we alternated the stimulation period with a control period to return the neuronal activation to its basal state. A paradigm contain a variety of tasks blocks or events, usually showing the same more than once to ensure a consistent BOLD response in the regions of interest [35].

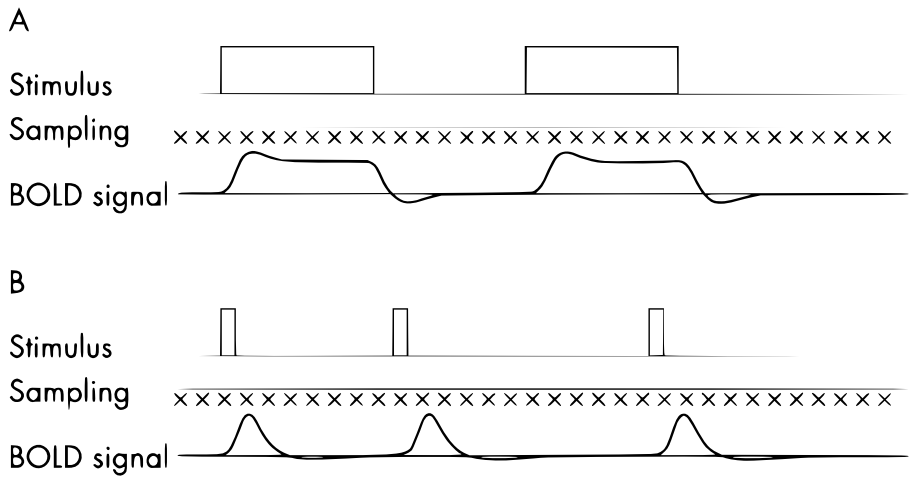

Figure 2.5: Block (A) and Event-related (B) paradigm designs [33]

Specific software for experimental design is needed to present these paradigms during the fMRI scan. There are a lot of software packages for fMRI study design and they differ in the way that stimuli are described: either via code or graphical interfaces. PsychoPy [39] is an example to specialized software to present stimuli from a paradigm to a subject. PsychoPy is a free suite of software tools written in Python designed to make the generation of experimental stimuli easier, using the latest advances in hardware and software. The software has a more logical and intuitive graphic interface for those who do not know how to program and also offers the possibility to describe all the experimental design in Python. This facilitates the management and creation of these paradigms by researchers in the areas of engineering and computing, who are the main ones responsible for this part.

2.4 Presurgical Planning using fMRI

The clinical applications of fMRI are still being explored by scientists and has a growing role in clinical neuroimaging [37]. An important clinical application of fMRI is to assist in neurosurgical planning, also called presurgical planning [52, 14]. Presurgical planning is a technique used for preoperative counseling to facilitates the evaluation of complex brain anatomy. In addition, it helps to analyze and speed up disease interpretation. In cases where the patient does not have metastases and the lesion, e.g. tumor, is considered small, there is the possibility of resecting the lesion through surgical intervention [41]. This is widely used in neurosurgery for patients with a brain tumor, vascular lesions, intractable temporal lobe epilepsy, and other resectable lesions [47, 6, 49].

The surgical treatment of brain tumors, for example, aims at the complete removal of the abnormality while minimizing the risk of inducing neurological deficits [49]. The localization of important cortical and subcortical areas at risk of injury during the surgical removal of resectable lesions is important to avoid permanent damage to neurological function [1, 46]. An example of this is shown in Figure 2.6. Figure 2.6*a* shows a T2-weighted images of a patient with a right parietal glioblastoma multiforme. The arrow points to the localization of the left central sulcus and the motor cortex. The location of these regions on the right hemisphere would coincide with the location of the tumor. Based on these images, the surgeon can infer that the lesion was inoperable. However, Figure 2.6*b* shows a fMRI activation during bilateral finger tapping. The T1-weighted images shows that the activation in the left hemisphere is located where it is anatomical expected. In right hemisphere the primary sensorimotor cortex has been displaced due to relocation of function, also known as cerebral plasticity. This cerebral plasticity is a response to pathology, where brain functions can be reallocated to other areas in the brain.

And this is an effect that, when identified by fMRI, can help to remove lesions without harming neurological functions.

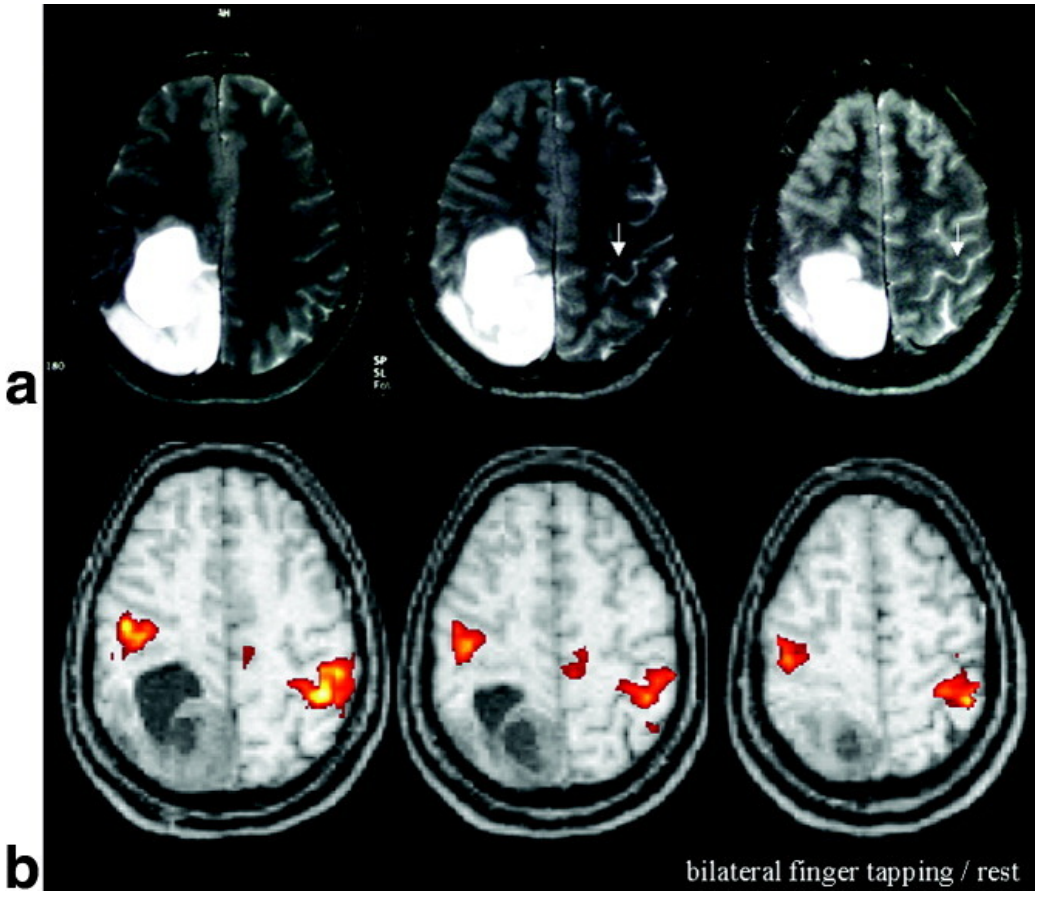

Figure 2.6: Analysis of a right parietal glioblastoma multiforme by T2-weighted images (*a*) and through brain activations obtained by fMRI (*b*) [49].

One of the most used tests for presurgical planning is the Wada test. The Intracarotid Amobarbital Test (IAT or Wada test) is universally relied on as a prognostic test for patients with intractable temporal lobe epilepsy who are candidates for neurosurgical intervention. The Wada test involves the temporary inactivation of one cerebral hemisphere by the injection of sodium amobarbital [1, 46] and has been used for more than half a century to determine language dominance. However, this test has a major shortcoming due to its invasiveness with a lack of standardization and absence of spatial resolution. Potential complications include encephalopathy, stroke, vessel dissection, and seizure [28]. By contrast, clinical usage of fMRI in presurgical planning is becoming a standard tool to avoid neurological impairment during surgery providing a finer spatial relationship between the lesion and brain functionality. fMRI maps brain areas involved in several functions, such as language and memory, and offers diagnostic information non-invasively before surgery and with justifiable clinical expenditure [50]. By using fMRI-based planning, a surgeon just needs to plan with an fMRI neuroscientist a paradigm with a set of stimuli. As fMRI is a repeatable procedure, it is advantageous to create validated paradigms to allow its use

instead of the Wada test. Using fMRI-based planning, the surgeon just needs to plan with an fMRI neuroscientist a paradigm with a set of stimuli.

As another example of the importance of presurgical planning, we brought one case report of an adolescent patient with an intractable epilepsy [42]. The patient had a left congenital temporal lobe tumor, a structural abnormality near cortical language areas. The clinical recommendation was for the removal of the tumor in hopes of achieving seizure control and without interfering with the neurologic and neuropsychological function. This patient underwent both Wada and fMRI procedures before the neurosurgical removal of the tumor. The fMRI was performed to determine the language dominance and lateralization of language functioning. Figure 2.7 shows the activations from a subvocal reading task, where the patient silently read short stories. The stories was four screens long and each screen was presented for 6 seconds. The figure shows the tumor, indicated by the arrow, the left-sided activation of frontal language areas (A) and right-sided activation of frontal and temporal language areas (B).

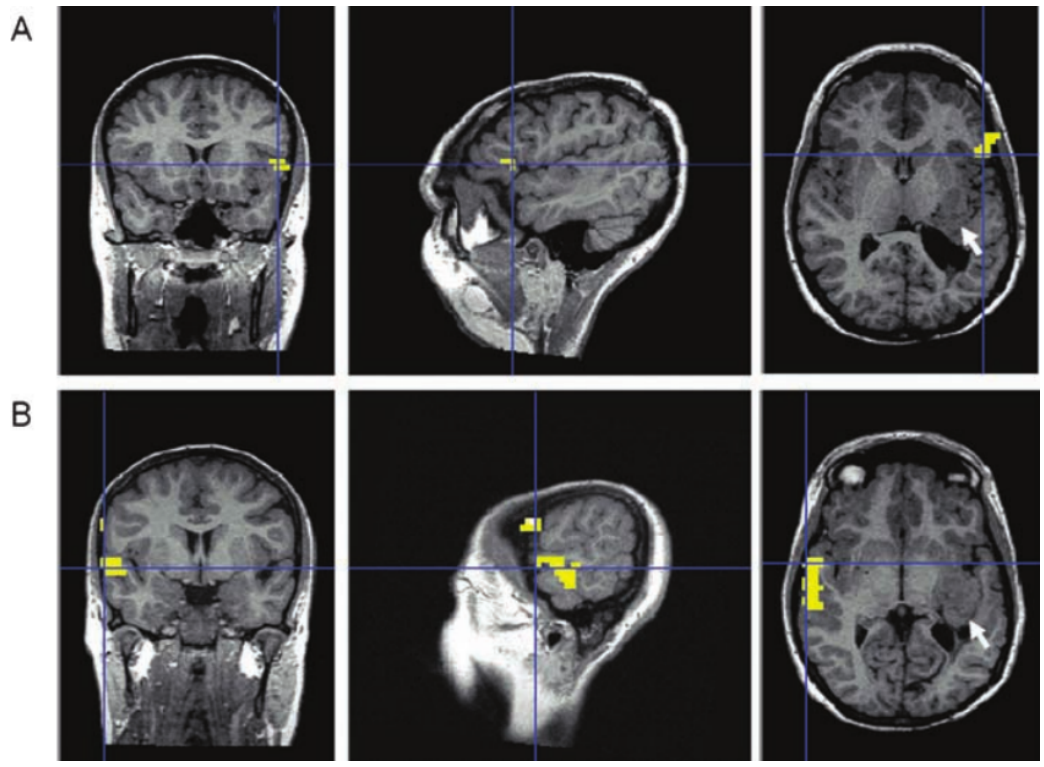

Figure 2.7: Presurgical example of brain activation during reading task on a clinical case. The tumor is indicated by the white arrow. [42]

Consistent with Wada and fMRI predictions, the removal of the mesial temporal tumor did not result in significant loss of language or verbal memory functioning. The assessment was made one year after the surgery, which was made with the preservation of left-sided cortical structures, like the hippocampus, amygdala, and parahippocampal gyrus. The Wada test failed to provide data about the localization of language function, just lateralization. This demonstrates the value of fMRI activity during language testing

and the potential of fMRI to provide new insights into brain functional organization for patients treated for epilepsy [42]. This case is another example of using fMRI for presurgical planning. The reported case uses a language paradigm already tested in other projects, as it activates a known and involved region with the tumor in question. However, when the cognitive functions of a region involved with the injury are not known, a larger study is needed to choose the paradigms. The development of an automatic tool for generating paradigms is necessary for cases lacking ready paradigms.

3. PLANNING BACKGROUND

In this chapter we present the theoretical framework necessary to understand the concepts of Automated Planning used throughout this work. Section 3.1 describes Automated Planning, an Artificial Intelligence subarea, and the Planning Domain Definition Language (PDDL) in Section 3.1.1. Section 3.1.2 briefly introduces the field of temporal numeric planner, that will be used in this work.

3.1 Automated Planning

Automated Planning is a subarea of Artificial Intelligence (AI) focused on developing formal languages and algorithms for the automatic generation of policies or plans of actions towards achieving specified goals. An AI planning system, or a *planner*, takes a domain model as input and uses some problem-solving technique, such as heuristic search, to work out its solution. This model describes the initial situation, the actions available to change it, and the goal condition to output a plan composed of those actions that will accomplish the goal when executed from the initial situation [22].

Planning algorithms are based on the *factored* transition function that represents states as discrete facts. While recent work tries to automatically derive this transition function [5] automatically, domain experts traditionally construct such transition functions manually. Automatically generating such domain knowledge involves at least two processes: converting real-world data into a factored representation and generating a transition function from traces of the factored representation.

In this work, we use the terminology from Ghallab et al. [15] as formalized by Pereira, Oren, and Meneguzzi [40] to represent planning domains and problems.

Definition 1 (*Predicates and state*)**.** *A predicate p represents logical values according to some interpretation as facts, which are divided into positive and negated facts, as well as constants for truth (T) and falsehood ($\bot$). A state $\mathcal{S}$ is a finite set of positive facts f that follows the closed world assumption so that if $f \in \mathcal{S}$, then f is true in $\mathcal{S}$.*

Definition 2 (*Actions*)**.** *An action a is a tuple $\langle name(a), pre(a), eff(a) \rangle$ where $name(a)$ is the name of the action, $pre(a)$ describe the preconditions of a (the set of predicates that must exist in the current state for a to be executed), and $eff(a)$ is the effect of a. The effects are divided into $eff(a)^+$ and $eff(a)^-$, for example, an add-list of positive predicates and a delete-list of negated predicates, respectively. An action a is applicable to a state $\mathcal{S}$ if and only if $\mathcal{S} \models pre(a)$ and generates a new state $\mathcal{S}'$ such that $\mathcal{S}' := (\mathcal{S} \cup eff(a)^+) / eff(a)^-$.*

Definition 3 (*Planning domain and instance*)**.** *A planning domain Ξ is represented by $\langle \Sigma, \mathcal{A} \rangle$: a finite set of facts Σ and a finite set of actions $\mathcal{A}$. The planning domains speci-*

fies the knowledge of the domain model. A planning instance comprises both a planning domain and the elements of a planning problem. The instance describes a finite set of objects of the environment, the initial state and the goal state which an agent wishes to achieve. A planning instance Π *is represented by a tuple* $\langle \Xi, \mathcal{I}, \mathcal{G} \rangle$*: the domain, initial and goal state definition. The initial state* $\mathcal{I}$ *is defined by specifying the value for all facts in the initial state. The goal state* $\mathcal{G}$ *represents a desired state to be achieved. Finally, a plan is a solution of a planning problem.*

Definition 4 (*Plan*)**.** *A plan* π *for a planning instance* $\Pi = \langle \Xi, \mathcal{I}, \mathcal{G} \rangle$ *is a sequence of actions* $\langle a_1, a_2, a_3, ..., a_n \rangle$ *that modifies the initial state* $\mathcal{I}$ *into a state* $\mathcal{S} \models \mathcal{G}$*. The goal state* $\mathcal{G}$ *is achieved by the successive execution of actions in a plan* π*. A plan* π^* *with length* $\mid \pi^* \mid$ *is optimal if there exists no other plan* π' *for* Π *such that* $\pi' < \pi^*$*. A plan* π *is considered optimal if its cost, and thus length, is minimal.*

3.1.1 Planning Domain Definition Language

The Planning Domain Definition Language (PDDL) is one problem description language to express planning models with a formal knowledge representation and is one of the most widely supported languages by planning systems. PDDL divides a planning problem into domain and problem definitions. The first defines the state variables that may be true or false and actions, while the second defines the initial state of the system and the goal that the plan must achieve. A domain in PDDL is described by **:requirements**, **:predicates**, and **:action**. The requirements indicates which features of PDDL the domain uses. The *predicates* (Definition 1) contains the list of the model's state variables. These are binary variables, representing facts that are either true or false. The *actions* that the planner can follow are described in Definition 2, and these define the transitions between states, the preconditions for the action to be performed, and its effects. The problem definition is described by **:objects**, **:init**, and **:goal**. The *objects* lists all of the objects in the problem instance. The initial state of this problem instance are defined in the *init*, by detailing all facts that are true in this state. The *goal* list the conjunction of facts that must be true for the goal to be achieved at the end of a valid plan. In summary, the domain describes the relevant aspects of the context in which it is being applied and the problem describes a specific situation that will be applied to this domain [22].

We exemplify PDDL use through a simple example of application: a switch example [22]. We have a switch that can be in two states, *on* and *off*, and we want to alternate between them. In this case, there are two possible actions to move the switch from one state to another. One action is for when the switch is *on*, and we want to turn it *off*. The other for when it's *off*, and we want to turn it *on*. To generate the plan for this switch example, we define that the switch is *on* in the initial state and our goal is to have the

switch *off*. Listing 3.1 shows the definition of the switch domain and Listing 3.2 of the switch problem in PDDL, based on the domain described.

```
(define (domain switch)
    (:requirements :strips)

    (:predicates (switch-is-on) (switch-is-off))

    (:action TurnOn
     :precondition  (switch-is-off)
     :effect (and   (switch-is-on)
                    (not (switch-is-off))
    )

    (:action TurnOff
     :precondition  (switch-is-on)
     :effect (and   (switch-is-off)
                    (not (switch-is-on))
    )
)
```

Listing 3.1: A domain definition for the switch example [22]

```
(define (problem turn_it_off)
    (:domain switch)
    (:init  (switch-is-on))
    (:goal  (switch-is-off))
)
```

Listing 3.2: A problem definition for the switch example [22]

The domain *switch* in Listing 3.1 introduces the two predicates that compose the set of states $\mathcal{S}$: *switch-is-on* and *switch-is-off*. We describe the two possible actions as: $a_1 = \langle TurnOn, OFF, (ON \cup \neg OFF)\rangle$ and $a_2 = \langle TurnOff, ON, (OFF \cup \neg ON)\rangle$. *ON* and *OFF* represents the *switch-is-on* and *switch-is-off* predicates, respectively. In the *turn-it-off* problem in Listing 3.2, we define that our current state $\mathcal{S}$ is the switch *on* and the goal $\mathcal{G}$ is to have the switch *off*. The planning instance to the switch domain is $\Pi = \langle switch, ON, OFF\rangle$. In this case, the plan π is the action $\pi = \langle TurnOff\rangle$.

3.1.2 Temporal Numeric Planning and PDDL+

Classical planning treats the time as relative [12] and takes into account only causal dependencies between actions (Definition 2). However, real-world problems often involve characteristics such as time, numbers, stochastic effects, and dynamic environments. These characteristics can be modeled using Temporal Numeric Planning. In temporal numeric planning, actions have duration, meaning that the effects are not always

applied instantly. The plan duration is expected to be as short as possible or to meet certain time constraints. Thus, plans can be generated with a greater number of actions, which is not a relevant metric for the quality of the plan [43].

Numeric planning extends classical planning with numeric state variables and uses languages such as PDDL 2.1 [12] and PDDL+ [13]. PDDL+ is the extension of PDDL for modeling hybrid systems through the use of *process* and *events* [22]. These formalisms allow modeling time-dependent change as instantaneous effects or as continuous change. A *process* act for an interval of time and have a continuous effect on numeric values. It corresponds to the definition of an action (Definition 2), but making it possible to include numerical effects. An *Event* is a discrete moment in time and the effects are only applied when the event's preconditions are met. For this project we use a simplification of PDDL+ formalism, adapting the terminology and the model introduced in Subsection 3.1.

Definition 5 (*Events*)**.** *We represent an event E as a tuple $\langle name(E), pre(E), eff(E)\rangle$ where $name(E)$ is the name of the event, $pre(E)$ describe the preconditions of E (the set of predicates that must exist in the current state for E to be executed), and $eff(E)$ is the effect of E. If an event's preconditions $pre(E)$ are satisfied, it occurs, yielding the event's instantaneous effects. The $eff(E)$ are the changes that take place in $\mathcal{S}'$ automatically once $pre(E)$ holds in $\mathcal{S}$.*

Definition 6 (*Processes*)**.** *We represent processes P likewise events, as a tuple $\langle name(P), pre(P), eff(P)\rangle$. The preconditions $pre(P)$ are the conditions for the process to continue. The $eff(P)$ are the changes that take place in $\mathcal{S}'$ automatically while $pre(P)$ holds in $\mathcal{S}$.*

Definition 7 (*PDDL+ Planning domain*)**.** *Finally, a PDDL+ planning domain $\Xi+$ is represented by $\langle \Sigma, \mathcal{A}, E, P\rangle$. We have a finite set of facts Σ, actions $\mathcal{A}$, events E, and processes P to modifies the initial state $\mathcal{I}$ into a state $\mathcal{S} \models \mathcal{G}$.*

.

We can use PDDL+ to model, for example, the drop of a ball to the ground. This is something that cannot be done with classical planning, but with temporal planning. In this case, we need to consider the action of gravity on the ball's fall and the speed at which it hits the ground. In addition to speed, it is necessary to consider the initial distance from the ground and the deceleration of the ball when bouncing. From the moment someone releases the ball, the *Falling* process begins (Listing 3.3), which has the effect of increasing the ball's speed according to gravity and decreasing the ball's distance from the ground.

When the distance from the ball to the ground is less than or equal to zero, no one is holding the ball, and the speed of the ball is greater than zero, this indicates that the ball has hit the ground. In this case, the *hit-ground* event is triggered (Listing), decreasing the ball's speed. In this *event* we considered that the speed of the ball was reduced by twenty percent, for example purposes only. This is just a simple example of using temporal planning with PDDL+.

```
(: process FALLING
    :parameters (?b - ball)
    :precondition (and
        (not (held ?b))
    )
    :effect (and
        (increase (velocity ?b) (* time 9.8))
        (decrease (distance-to-floor ?b) (* time (velocity ?b)))
    )
)
```

Listing 3.3: Process: FALLING

```
(: event HIT-GROUND
    :parameters (?b - ball)
    :precondition (and
        (not (held ?b))
        (<= (distance-to-floor ?b) 0)
        (> (velocity ?b) 0)
    )
    :effect (and
        (assign (velocity ?b) (* -0.8 (velocity ?b)))
    )
)
```

Listing 3.4: Event: HIT-GROUND

3.1.3 Expressive Numeric Heuristic Search Planner

The Expressive Numeric Heuristic Search Planner (ENHSP) [45, 44] is one PDDL automated planning system that supports several versions of PDDL, such as PDDL+. ENHSP is a forward heuristic search planner and transforms the PDDL into a graph-search problem. Nodes represent states visited by the planner and the search in the graph is guided by a heuristic function to explore only those nodes whose associated state is reachable from the initial state and reaches states closer to the goals.

4. MODELLING FMRI STUDIES IN PDDL+

In this Chapter, we detail our method to model fMRI studies using PDDL+. Section 4.1 briefly summarizes the paradigms used in this work and the demographic information of each one. Next, Section 4.2 details the analyses performed on the fMRI data to extract brain activation patterns for each paradigm. Section 4.3 introduces the PDDL+ representation of the fMRI paradigm planner.

4.1 Dataset Overview

We use the paradigms provided by the Brain Institute (BraIns) of Rio Grande do Sul (*Instituto do Cérebro do Rio Grande do Sul - INSCER*) to create the paradigm database. This dataset is composed of tasks that activate areas related to motor skills, language, visual, auditory, memory, attention, and default mode network. The BraIns dataset requires that the data be anonymized once the project is concluded to be made publicly available. We already have access to the anonymized version of the BraIns dataset. We use four different paradigms to extract information about brain activations. Table 4.1 presents the dataset demographic information for each paradigm P_x. The *Stimuli* column shows the total stimuli presented in the paradigm, followed by the number of fMRI data (subjects) for each paradigm, and the mean age and standard deviation SD of the population.

	Stimuli	Subjects	Mean Age (± SD)
P_1	60	46	9.83 ± 0.29 years
P_2	48	51	8.83 ± 0.35 years
P_3	60	100	9.41 ± 1.81 years
P_4	60	49	12 ± 1.02 years

Table 4.1: Dataset demographic information for each paradigm P_x

P_1 and P_2 are paradigms of mathematical reasoning. P_1 is a number sense paradigm, with two blocks of 5 seconds. Participants were shown 5 arithmetic equations in sequence (*e.g.* 8+1 = 9), followed by the presentation of 5 sets of numbers (*e.g.* [9 0 5 4 8]). The participant needs to select the set with the correct answers. Altogether, 30 equations and 30 responses are presented. Between each stimulus, a small interval between 0.5 and 1 second is shown. P_2 consists of 2 block stimuli: figure and response, of 6 and 3 seconds, respectively. First, a figure is presented with a basic math problem, followed by a response, that the participant must decide if is correct. Participants select “Yes” or “No” answers by pressing response buttons placed on both hands, with “Yes” on the left hand and “No” on the right, to match on-screen positions of those words. After the presentation of a figure and a response, there is a rest interval of 1 or 2 seconds, and every 16 stimuli

there is a rest interval of 30 seconds. In all, 24 figures and 24 different responses are presented. P_3 is a language paradigm that uses visual words stimuli. The paradigm contains 3 blocks of stimuli presented for 7 seconds each. Subjects are presented 20 words of each category: regular, irregular, and pseudo-words, totaling 60 words. For each word, the subject responds with buttons if the word presented exists or not. Figure 4.1 shows an example of the structure of the language paradigm.

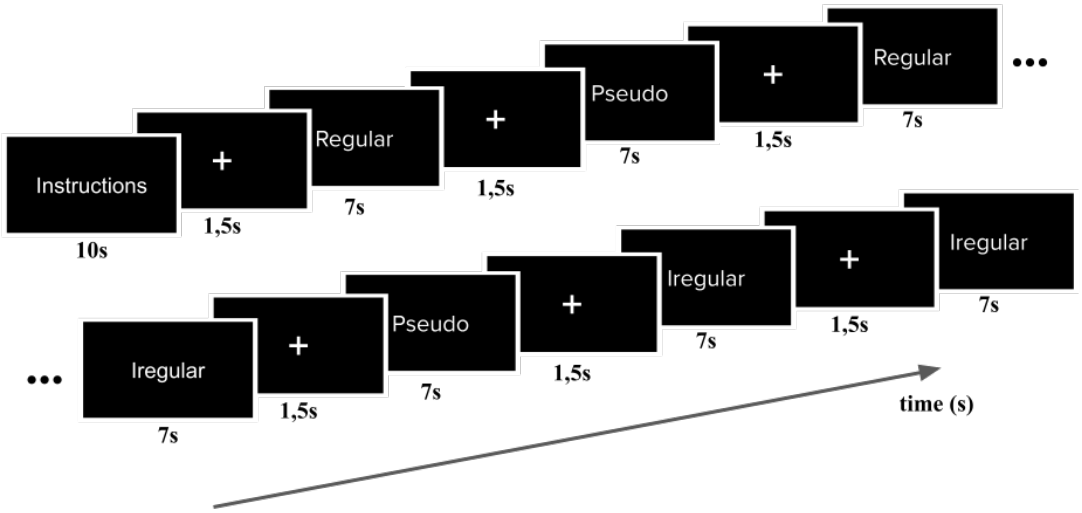

Figure 4.1: *P3*: Language paradigm example.

P_4 is a verbal memory task that uses lists of words that are always related to the same theme. Before the scan, the participants had access to this list for a certain time and, during the scan, they had to answer whether the projected words were present or not in the list. Therefore, this is a paradigm composed of two blocks of words (displayed for 2 seconds on the screen): true memories and false memories, 30 words of each.

All data was collected on a GE HDxT 3.0 T MRI scanner with an 8-channel head coil. The task EPI sequences used the following parameters: TR = 2000 ms, TE = 30 ms, 29 interleaved slices, slice thickness = 3.5 mm; slice gap = 0.1 mm; matrix size = 64 x 64, FOV = 220 x 220 mm, voxel size = 3.44 x 3.44 x 3.60 mm.

4.2 Extraction of Brain Activation Intensities

We need to identify the number of active voxels in the brain regions according to each stimulus presented. By knowing the regions activated by each stimulus our planner can select the right stimuli to achieve the goal set for the planner. For that, we chose to divide the brain according to a brain atlas, aiming at a better distribution of brain regions. The atlas used was from the Haskins Laboratory [34], which divides the brain into 107 regions considering laterality of each one. The Haskins pediatric atlas was generated from

72 children (aged 7-14 years) and was developed to improve labelling accuracy of anatomical and functional regions for MRI studies in children. Figure 4.2 shows the Haskins atlas in the three basic planes of MRI, with each color being one of the brain regions.

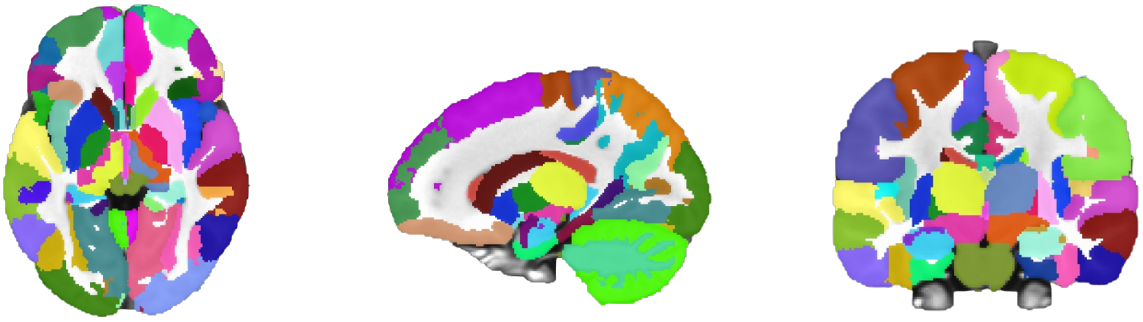

(a) Axial (b) Sagittal (c) Coronal

Figure 4.2: Haskins pediatric atlas on basic planes of MRI: axial, sagittal and coronal planes.

All our development work considers the brain regions of the atlas, numbered from 1 to 107. However, 21 of the 107 regions cannot be used because they are regions where there is no BOLD signal, such as the ventricles, for example. So we divide the brain into the 86 regions from Table 4.2 with their respective numbers and names. The table shows the number of the regions for the left and right cerebral hemisphere in the first and second columns respectively.

4.2.1 Gosset (Student) T-test

We run a group-level analysis to estimate the activation intensities evoked by each of block and event stimulus, using the `3dttest++` command in the Analysis of Functional NeuroImages (AFNI) software [9, 19]. The `3dttest++` is the Gosset (Student) t-test of sets of 3D datasets. AFNI computes the standard error and the mean for a contrast estimate. This contrast is the comparison of each task with the moment of rest to obtain the regions activated by the task. We obtained the average activation of the dataset for each stimulus from this analysis. This first analysis allows us to map the brain regions evoked in each stimulus. For example, side A of the Figure 4.3 shows the result of the average activations for a language stimulus for $p<0.001$. From the *ttest*, it is also possible to analyze the regions individually. Side B of the Figure 4.3 shows the activation cluster for the Left Insula with a size of 155 voxels. These voxels were obtained with the stimulus repeated 20 times, according to the original paradigm.

Left Side	Right Side	Region
6	24	Caudate
7	25	Putamen
8	26	Pallidum
12	27	Hippocampus
13	28	Amygdala
15	29	Accumbens
16	30	Ventral DC
17	31	Vessel
18	32	Choroid Plexus
40	74	Banks STS
41	75	Caudal Anterior Cingulate
42	76	Caudal Middle Frontal
43	77	Cuneus
44	78	Entorhinal
45	79	Fusiform
46	80	Inferior Parietal
47	81	Inferior Temporal
48	82	Isthmus Cingulate
49	83	Lateral Occipital
50	84	Lateral Orbitofrontal
51	85	Lingual
52	86	Medial Orbitofrontal
53	87	Middle Temporal
54	88	Parahippocampal
55	89	Paracentral
56	90	Pars Opercularis
57	91	Pars Orbitalis
58	92	Pars Triangularis
59	93	Pericalcarine
60	94	Postcentral
61	95	Posterior Cingulate
62	96	Precentral
63	97	Precuneus
64	98	Rostral Anterior Cingulate
65	99	Rostral Middle Frontal
66	100	Superior Frontal
67	101	Superior Parietal
68	102	Superior Temporal
69	103	Supramarginal
70	104	Frontal Pole
71	105	Temporal Pole
72	106	Transverse Temporal
73	107	Insula

Table 4.2: List of the 86 regions used in this work based on the Haskins Atlas.

Figure 4.3 clusters the regions with a minimum cluster size of 40 voxels, for illustration purposes. The minimum number of voxels in the cluster is defined individually

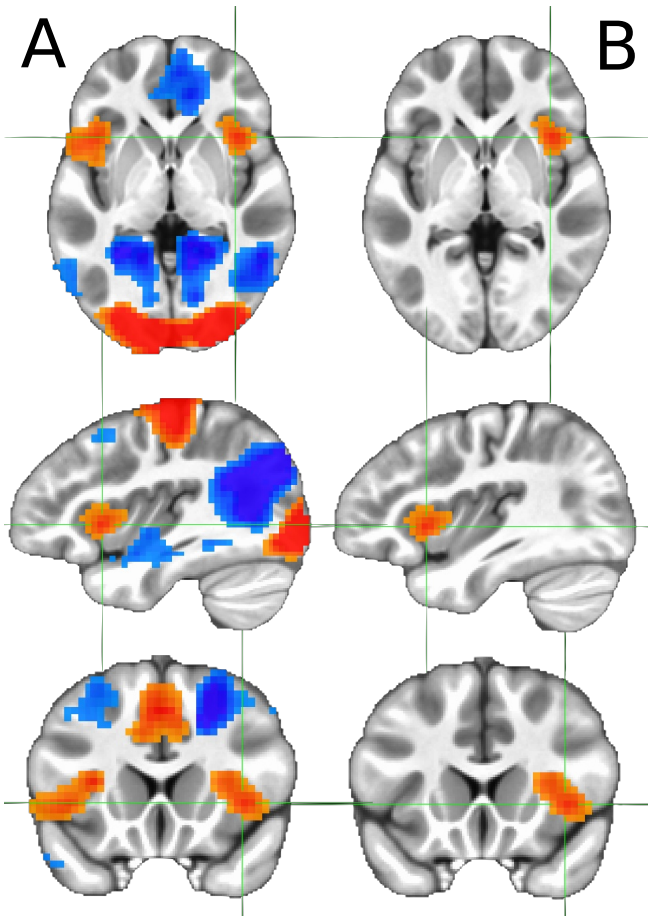

Figure 4.3: (A) Group-level analysis results for a language stimulus. (B) Right Insula: cluster with 155 voxels.

for each paradigm, indicating how many voxels are needed for an activation to be statistically significant. This procedure is called Correction for Multiple Comparisons and was performed from the `3dClustSim` command in AFNI. This command makes a correction for MRI false positives and calculates the number of voxels needed for each paradigm. The minimum cluster size obtained from the correction for multiple comparisons was: 55.7 voxels for P_1, 32 voxels for P_2, 59 voxels for P_3, and 33 voxels for P_4.

4.2.2 Region Of Interest Analysis

After the *ttest* we need to correlate the brain regions with the Haskins atlas and perform the count of active voxels in each of the regions. This correlation was made considering the Region of Interest Analysis (ROIs). We generated 107 NIfTI files using the *3dCalc* AFNI command, each representing one of the 107 Haskins atlas regions. NIfTI is the abbreviation of *Neuroimaging Informatics Technology Initiative* and is a data format for the storage of fMRI and other medical images. Figure 4.4 exemplifies the division of the Haskins Atlas into the Regions of Interest. The region pointed by the arrow (4.4a)

corresponds to ROI 63, the left precuneus. Figure 4.4b shows the same region separated from the others after *3dCalc* command.

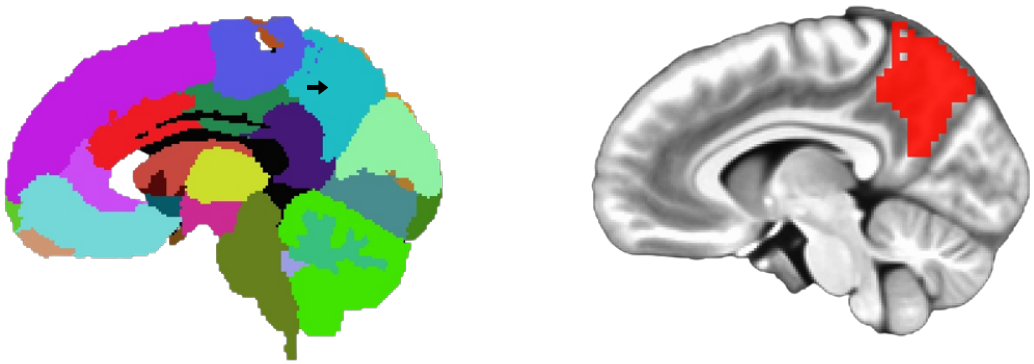

(a) Haskins Atlas (b) ROI 63

Figure 4.4: ROI example: (a) Atlas Haskins with ROI 63 pointed by the arrow. (b) ROI 63 obtained by *3dCalc* AFNI command.

With this regions separated, we can correlate each ROI with the brain activation files obtaneid by *ttest* (4.2.1). The count of active voxels for each of the regions of interest was performed using the *3dBrickStat* AFNI command. After these procedures, we have the activation value of each ROI for each of the stimuli used in this work. The values of ROIs activation are described in Table A in Appendix A.

4.3 Modelling fMRI Studies in PDDL+

In this section, we present the actual model of our PDDL+ representation of the fMRI paradigm planner problem. We derive planning domains representing the relation of stimuli in the fMRI paradigm with the various anatomic cerebral regions from Haskins Atlas (Table 4.2). Our model was based on the four paradigms described in the Section 4.1.

4.3.1 PDLL+ Representation: Domain and Instance

After extracting brain activation we describe fMRI studies using PDDL+. We create a predicate (Definition 1) representing the activation intensity of each region and a predicate to represent that the region is active. We also create a predicate representing the *instructions* and the *rest* intervals. Listing 4.1 shows a simplification of predicates written in PDDL+.

```
(:predicates
    (instructions)
    (rest)

    (intensity_ROI_1)
    (...)
    (intensity_ROI_107)

    (active_ROI_1)
    (...)
    (active_ROI_107)
)
```

Listing 4.1: Predicates PDDL+

All fMRI experiments begin with an instruction screen, presented to prepare the subject for the performed paradigm. The instructions were modeled as a single *action* $\langle BeginExperiment, \{\neg instructions\}, \{(time \leftarrow time + 10), instructions, \neg rest\}\rangle$, executed in the beginning of all experiments. The time is increased by 10 seconds, which is the usual block time for instructions.

Key to our modeling of the paradigms is predicting neural activation in the regions of interest for the study at hand. Thus, we represent each planner *action* that describes the fMRI stimuli as $\langle Stimulus(ST), \{rest, instructions\}, \{actived(R), (intensity(R) \leftarrow intensity(R) + X), (time \leftarrow time + Y), \neg rest\}\rangle$, where R is a vector of regions activated by the stimulus ST, X is the activation intensity of each ROI R and Y is the time that the block or event B is displayed on the screen. Listing 4.1 shows an example of action written in PDDL+.

```
(:action Stimulus(ST)
    :parameters (?t - timing)
    :precondition (and
        (instructions) (rest))
    :effects (and
        (active_ROI_6)
        (increase (intensity_ROI_6) 2.35)
        (active_ROI_7)
        (increase (intensity_ROI_7) 7.9)
        (...)
        (increase (total ?t) 7)
        (not (rest)))
)
```

Listing 4.2: Problem Domain PDDL+ - Action Example

Between the presentation of the stimuli, small rest intervals are presented. These usually last 1 to 2 seconds and were modeled as *actions* $\langle BaselineRest, \neg rest \wedge instructions, (intensity(R) \leftarrow intensity(R) - X) \wedge (time \leftarrow time + Y) \wedge rest\rangle$. In this case, R is a vector

of all brain regions, and the rest intervals result in a decrease of X units in the activation intensity in all brain regions. We model long rest intervals during the experiment as *events* (Definition 5), allowing the neuronal activation to return to its basal state. The baseline *event* is represented by a tuple $\langle(time = W), (intensity(R) \leftarrow intensity(R) - X) \wedge (time \leftarrow time{+}30)\rangle$. The baseline event happens when the total time of the experiment reaches time W.

The PDDL+ instance was described as $\langle(intensity(R) = 0), (\neg(actived(R)), rest, \neg instructions\rangle$. We initialize activation intensities of brain regions to zero and that the regions are not active. We set the experiment time to zero, the experiment at rest, and the instructions are not on the screen. This is described in Listing 4.3.

```
(:init
    (rest)
    (not (instructions))
    (= (total experiment_time) 0)
    (= (intensity_ROI_1) 0)
    (...)
    (= (intensity_ROI_107) 0)
    (not (active_ROI_1))
    (...)
    (not (active_ROI_107))
)
```

Listing 4.3: Problem Instance PDDL+ - Init

The planner *goals* were defined as $\langle active(R), (time >= min), (time <= max)\rangle$. The goal is composed of the regions to be activated and the paradigm's time limits. We put the minimum and maximum experiment time as goal as this is an important variable when planning the paradigms to reduce the scan cost. We use the metric *maximize* as $\langle intensity(R)\rangle$ to maximize the activation intensity of the brain regions settled as the goal.

```
(:goal
    (and
        ; Set minimum experiment time (seconds)
        (>= (total experiment_time) 100)
        ; Set maximum total experiment time (seconds)
        (<= (total experiment_time) 200)
        ; Set Regions of Interest (ROIs)
        (active_ROI_106)
    )
)
; Set ROIs to maximize intensity
(:metric maximize (intensity_ROI_106))
```

Listing 4.4: Problem Instance PDDL+ - Goal

5. RESULTS

We develop a Shell script in *bash* to unify the planning process. The script reads the domain and the instance in PDDL+ and sends to ENHSP. The ENHSP allows you to choose specific setting as search engine (*e.g.*sat and opt). *Sat* and *opt* are the configurations for the satisficing and the optimal version of ENHSP. All the results presented were considering the optimal planning as default, but the script presents the other available options of search engine. The script calls ENHSP that plans the paradigm according to the goals defined in the instance problem, saving in a text file. After generating the stimulus sequence, we convert it so that it can be presented to the subject during the MRI scan. To present such paradigm, our script uses the Psychopy software and generates the corresponding paradigm from the *csv* file, being ready to be used during the fMRI exam.

We test two scenarios by changing the ROIs to be actived and verifying the activation resulting from the generated paradigm. In the first scenario, presented in List 5.1 we defined ROI 94 (Right Postcentral) as a goal and that the paradigm should be between 1 and 1.5 minutes long.

```
(:goal
    (and
        (>= (total experiment_time) 60)
        (<= (total experiment_time) 90)
        (active_ROI_94)
    )
)
(:metric maximize (intensity_ROI_94))
```

Listing 5.1: First Scenario - ROI 94

The paradigm generated was the $P4$ (Section 4.1), a verbal memory task, composed of 8 *true memories* and 5 *false memories*, of 2 seconds each. In addition to these, the paradigm was composed of an *instruction* block (10 seconds) and 14 *rest* blocks (1.75 seconds each), totalizing 60.5 seconds of paradigm. Figure 5.1 shows the ROI 94 localization in brain atlas blue painted (Figure 5.1a) and the resulting activations from this paradigm red painted (Figure 5.1b).

In the second scenario we defined ROIs 66 (Left Superior Frontal) and 85 (Right Lingual) as the goals and that the paradigm should be between 5 and 6 minutes long. The paradigm generated was the $P3$ (Section 4.1), a verbal language paradigm, composed of 8 *regular words*, 13 *irregular words* and 12 *pseudo words*, of 7 seconds each. In addition to these, the paradigm was composed of an *instruction* block (10 seconds) and 34 *rest* blocks (1.75 seconds each), totalizing 300.5 seconds of paradigm, just over 5 minutes. Figure 5.2 shows the ROI 66 localization in brain atlas blue painted (Figure 5.2a), the ROI 85 localization blue painted (Figure 5.2b), and the resulting activations from this paradigm

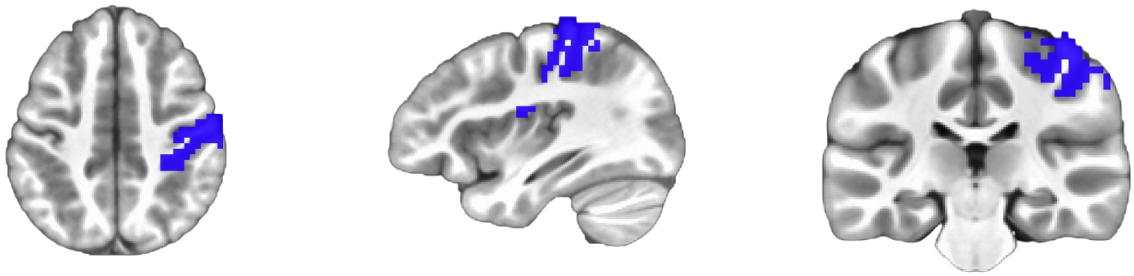

(a) ROI 94

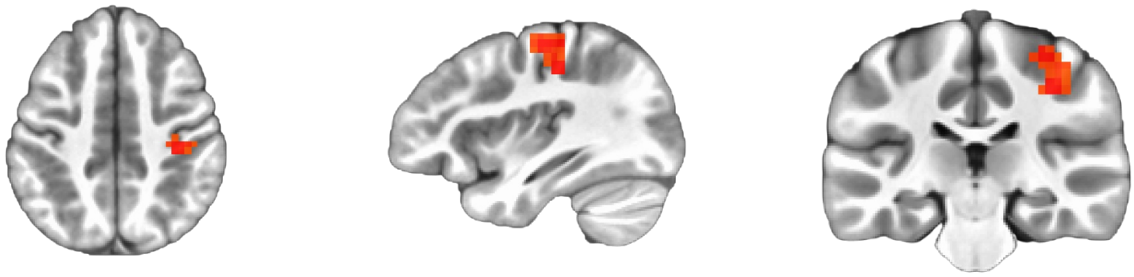

(b) Resulting brain activation

Figure 5.1: Planned paradigm results for ROI 94, the Right Postcentral, as planner's goal. The location of ROI 94 in the brain is painted blue *(a)*. The activations resulting from the paradigm planned in the first scenario (1-2 minutes as experiment time) is red painted *(b)*.

red painted (Figure 5.2c). With this examples we can confirm that the planner generates paradigms according to the defined goal.

The main contribution of this work is an automatic mechanism that allows a surgeon to assess cognitive activities related to areas at risk of injury during the surgical removal of brain tumors or resectable lesions. As an example of the importance of presurgical planning, we use the case report of an adolescent patient with an intractable epilepsy [42], presented in the Section 2.4. The patient had a left congenital temporal lobe tumor, a structural abnormality near cortical language areas. We compare our presurgical planning domain with the results obtained by the actual fMRI scan used for presurgical planning of the Chapter 2.4, shown in Figure 2.7.

In order to generate the paradigm for the fMRI presurgical planning, we set ROI 58 (Left Pars Triangularis) as the planner's goal. The Left Pars Triangularis is the triangular shaped cortical region of the Left Interior Frontal Gyrus (LIFG). LIFG plays a key role in the cerebral cortical network that supports reading and visual word recognition [8]. We chose this region because it is one of the regions responsible for language processing, comprehension, and production [32]. The paradigm obtained by the planner is a language paradigm that uses visual words stimuli. For each word, the subject responds with buttons

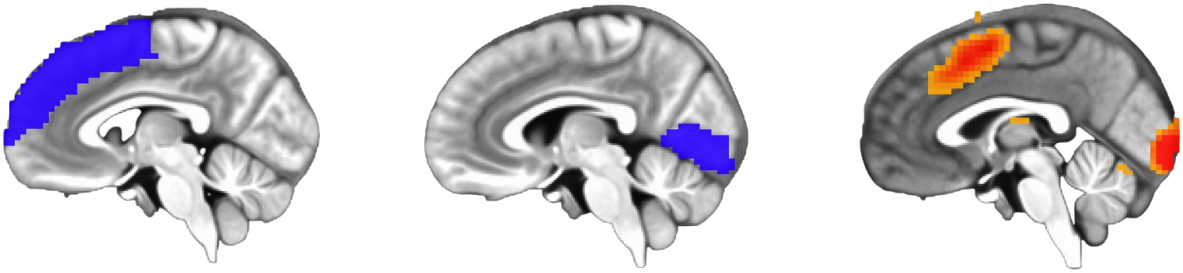

(a) ROI 66 (b) ROI 85 (c) Activations

Figure 5.2: Planned paradigm results for ROIs 66 and 85 as planner's goal. The location of ROI 66 in the brain is painted blue *(a)*. The location of ROI 85 in the brain is painted blue *(b)*. The activations resulting from the paradigm planned in the second scenario (5-6 minutes as experiment time) is red painted *(c)*.

if the word presented exists or not. Figure 5.3 shows the brain activations of our planned paradigm.

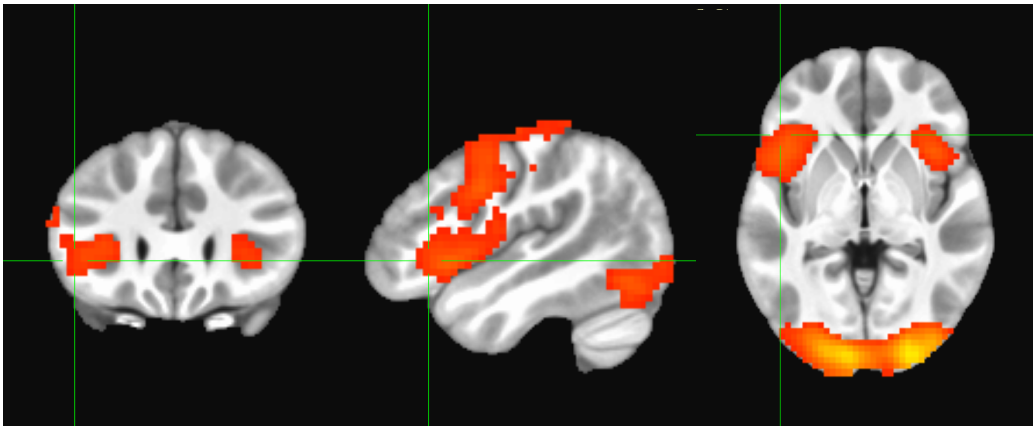

Figure 5.3: Comparison of the results of the presurgical planning described in Figure 2.7 with the results of our paradigm planner. Brain's activations for the paradigm planned to ROI 58 as planner's goal (a).

The cursor points to activation in the LIFG region and a right-sided activation of frontal language areas and occipital lobe activation can also be observed in the figure. The presence of occipital activation is common because it is a region of the visual cortex. Consistent with Wada, fMRI predictions, and our fMRI paradigm planner, the removal of the mesial temporal tumor did not result in significant loss of language or verbal memory functioning. This demonstrates the value of fMRI activity during language testing and the potential of fMRI to provide new insights into brain functional organization for patients treated for epilepsy [42]. The paradigm planned by our domain obtained results very similar to those obtained in the fMRI exam carried out in this clinical study.

6. RELATED WORK

Recent approaches [4, 2, 5] use neural-networks to automatically generate domain models from images. These neural networks convert an input image into a discretized representation, which can stand for the logical fluents used in planning. This obviates the need for a domain expert, and turns the problem of planning domain design into a data-driven one. This is especially important for domains involving real-world phenomena that need to be captured in fine detail, as is the case for fMRI paradigm design.

Previous work shows the difficulty of modeling the BOLD signal. [31] study attempted a Bayesian estimation of the cerebral Hemodynamic Response. This is a way to analyze BOLD fMRI data considering the whole brain as a system. This system is characterized by a transfer response function, called the Hemodynamic Response Function (HRF). After extensive research and mathematical modeling, they proved that, in real data, a wide variety of HRF forms are found. This shows that there is still more to investigate and much research to be done. We found several studies on this type of modeling, but with unsatisfactory results. We have not found related work suitable as a basis for the application of automated planning to paradigm design. In this way, our work is the first to attempt to model fMRI paradigms using automated planning.

7. CONCLUSION

We developed an application of PDDL+ to planning neuroimaging paradigms to solve the dual problem of effective paradigm design and scan cost minimization. Empirical experimentation shows that our planner successfully generates a valid presurgical planning paradigm that approximates the activations expected of a manually designed paradigm. Our planner was developed to create paradigms within the time frame that the user defines and, in that time, maximize the intensity of each region.

Our first ideas and approaches involved the research of mathematical modeling of the BOLD signal. Mathematical signal modeling is still an emerging area of research, widely studied and with many different approaches [18, 48, 20]. The latest [20] uses a model-based Reinforcement Learning technique for systems with non-Markovian dynamics, as BOLD signal. One of the works used to study mathematical modeling [31] shows that even with an efficient framework, BOLD signal curves in real life are very different. To work with the BOLD signal and try to predict exact activation values, our database would need many images of different ages and populations. As this is an extremely complex job and would demand a much larger dataset and more research time, we chose to work with average values. Therefore, we decided to use the mean values approach, based on the *ttests* that were done. Previously, we used empirical values and now, values that correspond to reality.

The final version of our paradigm planner uses values of brain activation intensity based on data from four different functional magnetic resonance paradigms. Our planner still has some limitations, such as the number of paradigms included and the age range of the participants used. We only use data from children, as this was the only extensive enough dataset we had access to, but we are confident our approach can be used for any other populations. By expanding the amount of data and stimulus options, our tool will become much more complete and effective.

We initially propose to solve the dual problem of effective paradigm design and scan cost minimization. Our work asks the user to define the minimum and maximum times that the paradigm should take in the scanner and also which regions should be active. Planning with a pre-defined time is important to try to minimize the cost of a scan, which is proportional to the time within the fMRI scanner. Thus, the planner seeks a paradigm, at the pre-defined time, to activate the defined regions and maximize their intensity.

There is still much research to be done in this area and our work is the first to attempt to use this type of approach in an fMRI context. We published our initial results in the 31st International Conference on Automated Planning and Scheduling (ICAPS) [11]. We have recently submitted a more complete version of this work to a journal and expect

to publish it within a year. In conclusion, our approach provides the basis for using automated planning in the context of designing fMRI paradigms. Moving forward, we expect this application to become a useful tool for Neuroscientific research and as a supporting resource for presurgical planning.

REFERENCES

[1] Acharya, J. N.; Dinner, D. S. “Use of the intracarotid amobarbital procedure in the evaluation of memory”, *Journal of Clinical Neurophysiology*, vol. 14–4, 1997, pp. 311–325.

[2] Amado, L. R.; Meneguzzi, F. “LatRec: Recognizing Goals in Latent Space”. In: Proceedings of the 34th AAAI Conference on Artificial Intelligence, 2020, pp. 13747–13748.

[3] Amaro Jr, E.; Barker, G. J. “Study design in fMRI: basic principles”, *Brain and Cognition*, vol. 60–3, 2006, pp. 220–232.

[4] Asai, M.; Fukunaga, A. “Classical Planning in Deep Latent Space: Bridging the Subsymbolic-Symbolic Boundary”. In: Proceedings of the 32nd AAAI Conference on Artificial Intelligence, 2018, pp. 6094–6101.

[5] Asai, M.; Muise, C. “Learning neural-symbolic descriptive planning models via cube-space priors: The voyage home (to STRIPS)”. In: Proceedings of the 29th International Joint Conference on Artificial Intelligence, IJCAI 2020, 2020, pp. 2676–2682.

[6] Benjamin, C. F.; Li, A. X.; Blumenfeld, H.; Constable, R. T.; Alkawadri, R.; Bickel, S.; Helmstaedter, C.; Meletti, S.; Bronen, R.; Warfield, S. K.; et al.. “Presurgical language fMRI: Clinical practices and patient outcomes in epilepsy surgical planning”, *Human Brain Mapping*, vol. 39–7, 2018, pp. 2777–2785.

[7] Buchweitz, A.; Costa, A. C.; Toazza, R.; de Moraes, A. B.; Cara, V. M.; Esper, N. B.; Aguzzoli, C.; Gregolim, B.; Dresch, L. F.; Soldatelli, M. D.; et al.. “Decoupling of the occipitotemporal cortex and the brain’s default-mode network in dyslexia and a role for the cingulate cortex in good readers: a brain imaging study of brazilian children”, *Developmental europsychology*, vol. 44–1, 2019, pp. 146–157.

[8] Cornelissen, P. L.; Kringelbach, M. L.; Ellis, A. W.; Whitney, C.; Holliday, I. E.; Hansen, P. C. “Activation of the left inferior frontal gyrus in the first 200 ms of reading: evidence from magnetoencephalography (MEG)”, *PloS one*, vol. 4–4, 2009, pp. e5359.

[9] Cox, R. W.; Hyde, J. S. “Software tools for analysis and visualization of fmri data”, *NMR in Biomedicine: An International Journal Devoted to the Development and Application of Magnetic Resonance In Vivo*, vol. 10–4-5, 1997, pp. 171–178.

[10] DeYoe, E. A.; Bandettini, P.; Neitz, J.; Miller, D.; Winans, P. “Functional magnetic resonance imaging (FMRI) of the human brain”, *Journal of Neuroscience Methods*, vol. 54–2, 1994, pp. 171–187.

[11] Esper, K. B.; Meneguzzi, F. “Automated design of fMRI paradigms”. In: Proceedings of the 31st International Conference on Automated Planning and Scheduling, 2021, pp. 445–449.

[12] Fox, M.; Long, D. “PDDL2.1: An extension to PDDL for expressing temporal planning domains”, *Journal of Artificial Intelligence Research*, vol. 20, 2003, pp. 61–124.

[13] Fox, M.; Long, D. “Modelling mixed discrete-continuous domains for planning”, *Journal of Artificial Intelligence Research*, vol. 27, 2006, pp. 235–297.

[14] Ganslandt, O.; Nimsky, C.; Buchfelder, M.; Grummich, P. “fMRI in Neurosurgery”. New York, NY: Springer New York, 2016, vol. 119, pp. 801–815.

[15] Ghallab, M.; Nau, D.; Traverso, P. “Automated planning and acting”. England: Cambridge University Press, 2016.

[16] Glover, G. H. “Deconvolution of impulse response in event-related BOLD fMRI”, *Neuroimage*, vol. 9–4, 1999, pp. 416–429.

[17] Glover, G. H. “Overview of functional magnetic resonance imaging”, *Neurosurgery Clinics*, vol. 22–2, 2011, pp. 133–139.

[18] Goense, J.; Bohraus, Y.; Logothetis, N. K. “fMRI at high spatial resolution: implications for BOLD-models”, *Frontiers in Computational Neuroscience*, vol. 10, 2016, pp. 66.

[19] Gold, S.; Christian, B.; Arndt, S.; Zeien, G.; Cizadlo, T.; Johnson, D. L.; Flaum, M.; Andreasen, N. C. “Functional MRI statistical software packages: a comparative analysis”, *Human brain mapping*, vol. 6–2, 1998, pp. 73–84.

[20] Gupta, G.; Yin, C.; Deshmukh, J. V.; Bogdan, P. “Non-markovian reinforcement learning using fractional dynamics”. In: Proceedings in the 60th IEEE Conference on Decision and Control (CDC), 2021, pp. 1542–1547.

[21] Hadjikhani, N.; Joseph, R. M.; Snyder, J.; Chabris, C. F.; Clark, J.; Steele, S.; McGrath, L.; Vangel, M.; Aharon, I.; Feczko, E.; et al.. “Activation of the fusiform gyrus when individuals with autism spectrum disorder view faces”, *Neuroimage*, vol. 22–3, 2004, pp. 1141–1150.

[22] Haslum, P.; Lipovetzky, N.; Magazzeni, D.; Muise, C. “An introduction to the planning domain definition language”. USA: Morgan & Claypool Publishers, 2019, vol. 13.

[23] Heinsfeld, A. S.; Franco, A. R.; Craddock, R. C.; Buchweitz, A.; Meneguzzi, F. “Identification of autism spectrum disorder using deep learning and the ABIDE dataset”, *NeuroImage: Clinical*, vol. 17, 2018, pp. 16–23.

[24] Huettel, S. A.; Song, A. W.; McCarthy, G.; et al.. “Functional magnetic resonance imaging”. USA: Sinauer Associates Sunderland, 2004, vol. 1.

[25] James, J. S.; Rajesh, P.; Chandran, A. V.; Kesavadas, C. “fMRI paradigm designing and post-processing tools”, *The Indian Journal of Radiology & Imaging*, vol. 24–1, 2014, pp. 13–21.

[26] Kirschner, M.; Sladky, R.; Haugg, A.; Stämpfli, P.; Jehli, E.; Hodel, M.; Engeli, E.; Hösli, S.; Baumgartner, M. R.; Sulzer, J.; et al.. “Self-regulation of the dopaminergic reward circuit in cocaine users with mental imagery and neurofeedback”, *EBioMedicine*, vol. 37, 2018, pp. 489–498.

[27] Lee, M. H.; Smyser, C. D.; Shimony, J. S. “Resting-state fMRI: a review of methods and clinical applications”, *American Journal of neuroradiology*, vol. 34–10, 2013, pp. 1866–1872.

[28] Loddenkemper, T.; Morris, H. H.; Möddel, G. “Complications during the Wada test”, *Epilepsy & Behavior*, vol. 13–3, 2008, pp. 551–553.

[29] Logothetis, N. K. “What we can do and what we cannot do with fMRI”, *Nature*, vol. 453–7197, 2008, pp. 869–878.

[30] Logothetis, N. K.; Wandell, B. A. “Interpreting the BOLD signal”, *Annu. Rev. Physiol.*, vol. 66, 2004, pp. 735–769.

[31] Marrelec, G.; Benali, H.; Ciuciu, P.; Poline, J.-B. “Bayesian estimation of the hemodynamic response function in functional MRI”. In: AIP Conference Proceedings, 2002, pp. 229–247.

[32] Marslen-Wilson, W. D.; Tyler, L. K. “Morphology, language and the brain: the decompositional substrate for language comprehension”, *Philosophical Transactions of the Royal Society B: Biological Sciences*, vol. 362–1481, 2007, pp. 823–836.

[33] Matthews, P. M.; Jezzard, P. “Functional magnetic resonance imaging”, *Journal of Neurology, Neurosurgery & Psychiatry*, vol. 75–1, 2004, pp. 6–12, https://jnnp.bmj.com/content/75/1/6.full.pdf.

[34] Molfese, P. J.; Glen, D.; Mesite, L.; Cox, R. W.; Hoeft, F.; Frost, S. J.; Mencl, W. E.; Pugh, K. R.; Bandettini, P. A. “The haskins pediatric atlas: a magnetic-resonance-imaging-based pediatric template and atlas”, *Pediatric Radiology*, vol. 51–4, 2021, pp. 628–639.

[35] Newman, S. D.; Twieg, D. B.; Carpenter, P. A. “Baseline conditions and subtractive logic in neuroimaging”, *Human Brain Mapping*, vol. 14–4, 2001, pp. 228–235.

[36] Ogawa, S.; Lee, T.-M. “Magnetic resonance imaging of blood vessels at high fields: in vivo and in vitro measurements and image simulation”, *Magnetic Resonance in Medicine*, vol. 16–1, 1990, pp. 9–18.

[37] Orringer, D.; Vago, D.; Golby, A. “Clinical applications and future directions of functional MRI”, *Seminars in neurology*, vol. 32, 09 2012, pp. 466–75.

[38] Pauling, L.; Coryell, C. D. “The magnetic properties and structure of hemoglobin, oxyhemoglobin and carbonmonoxyhemoglobin”, *Proceedings of the National Academy of Sciences*, vol. 22–4, 1936, pp. 210–216.

[39] Peirce, J. W. “Psychopy—psychophysics software in python”, *Journal of Neuroscience Methods*, vol. 162–1-2, 2007, pp. 8–13.

[40] Pereira, R. F.; Oren, N.; Meneguzzi, F. “Landmark-based approaches for goal recognition as planning”, *Artificial Intelligence*, vol. 279, 2020, pp. 32.

[41] Petrella, J. R.; Shah, L. M.; Harris, K. M.; Friedman, A. H.; George, T. M.; Sampson, J. H.; Pekala, J. S.; Voyvodic, J. T. “Preoperative functional mr imaging localization of language and motor areas: effect on therapeutic decision making in patients with potentially resectable brain tumors”, *Radiology*, vol. 240–3, 2006, pp. 793–802.

[42] Ries, M. L.; Boop, F. A.; Griebel, M. L.; Zou, P.; Phillips, N. S.; Johnson, S. C.; Williams, J. P.; Helton, K. J.; Ogg, R. J. “Functional MRI and Wada determination of language lateralization: a case of crossed dominance”, *Epilepsia*, vol. 45–1, 2004, pp. 85–89.

[43] Rintanen, J. “Complexity of concurrent temporal planning”. In: Proceedings of the 17th International Conference on Automated Planning and Scheduling, 2007, pp. 280–287.

[44] Scala, E.; Haslum, P.; Magazzeni, D.; Thiébaux, S. “Landmarks for numeric planning problems.” In: Proceedings of the 26th International Joint Conference on Artificial Intelligence, IJCAI 2017, 2017, pp. 4384–4390.

[45] Scala, E.; Haslum, P.; Thiébaux, S.; Ramirez, M. “Interval-based relaxation for general numeric planning”. In: Proceedings of the 22th European Conference on Artificial Intelligence, ECAI 2016, 2016, pp. 655–663.

[46] Sharan, A.; Ooi, Y. C.; Langfitt, J.; Sperling, M. R. “Intracarotid amobarbital procedure for epilepsy surgery”, *Epilepsy & Behavior*, vol. 20–2, 2011, pp. 209–213.

[47] Shimony, J. S.; Zhang, D.; Johnston, J. M.; Fox, M. D.; Roy, A.; Leuthardt, E. C. “Resting-state spontaneous fluctuations in brain activity: a new paradigm for presurgical planning using fMRI”, *Academic Radiology*, vol. 16–5, 2009, pp. 578–583.

[48] Sten, S.; Lundengård, K.; Witt, S. T.; Cedersund, G.; Elinder, F.; Engström, M. “Neural inhibition can explain negative bold responses: a mechanistic modelling and fMRI study”, *Neuroimage*, vol. 158, 2017, pp. 219–231.

[49] Sunaert, S. “Presurgical planning for tumor resectioning”, *Journal of Magnetic Resonance Imaging: An Official Journal of the International Society for Magnetic Resonance in Medicine*, vol. 23–6, 2006, pp. 887–905.

[50] Tieleman, A.; Deblaere, K.; Van Roost, D.; Van Damme, O.; Achten, E. “Preoperative fMRI in tumour surgery”, *European Radiology*, vol. 19–10, 2009, pp. 2523–2534.

[51] Toazza, R.; Franco, A. R.; Buchweitz, A.; Molle, R. D.; Rodrigues, D. M.; Reis, R. S.; Mucellini, A. B.; Esper, N. B.; Aguzzoli, C.; Silveira, P. P.; Salum, G. A.; Manfro, G. G. “Amygdala-based intrinsic functional connectivity and anxiety disorders in adolescents and young adults”, *Psychiatry Research: Neuroimaging*, vol. 257, 2016, pp. 11–16.

[52] Vlieger, E.-J.; Majoie, C. B.; Leenstra, S.; Den Heeten, G. J. “Functional magnetic resonance imaging for neurosurgical planning in neurooncology”, *European Radiology*, vol. 14–7, 2004, pp. 1143–1153.

APPENDIX A – ROIS ACTIVATION VALUES

ROI	E1	E2	E3	E4	E5	E6	E7	E8	E9
6	0.85	0.7	2.35	0.73	2.57	0	0.08	0.03	0.03
7	0.4	0.1	7.9	1.13	0.6	0	0.04	0	0
8	0.1	0	0.95	0.4	0.7	0	0	0	0
12	0.8	0.6	2.75	5.4	3.23	1.25	1.75	0	0
13	0	0	0	1.46	0.23	0.17	0.04	0	0
14	0.5	0.15	0.65	1.2	1.53	0	0.08	0	0
15	0.45	0	0.65	0.46	0.47	0	0	0	0.1
16	0.6	0	1.4	1.1	2.13	0	0	0	0.03
17	0	0	0	0	0	0	0	0	0
18	0.05	0	0	0.03	0.07	0	0	0	0.03
24	1	0.3	3.65	2.83	4.53	1.46	0.58	0	0.1
25	0.15	0.25	1.65	2.7	1.97	0.37	1	0	0.5
26	0	0	0.4	0.6	1.2	0.08	0	0	0
27	1.35	2.45	4.2	5.76	4.53	1.17	0.12	0	0
28	0.05	0.2	0.95	1.53	0.47	0.79	0	0	0
29	0.45	0.2	1.35	0.9	0.73	0	0	0	0.23
30	0.05	0	0.45	2.83	2.57	0.04	0	0	0.03
31	0	0	0	0.06	0	0	0	0	0
32	0	0	0.05	0.23	0.23	0	0	0	0.1
40	4.8	4.85	6.95	3.3	2.53	0.29	8.67	6.13	6.5
41	4.15	3.1	4.75	0.1	0.63	2.37	4.17	0.53	0.83
42	15.5	15.8	24.6	5.53	7.13	7.95	8.70	2.53	3.1
43	18.75	18.1	18.1	11.53	11.67	7.17	6.17	1	1.9
44	0.1	0	0.95	3	2.03	0.08	0.58	0	0
45	18.85	19	24.95	5	4.73	6.67	13.25	0.7	0.5
46	44.5	45.55	50.85	21.93	18.37	14.25	11.70	0	0
47	3.65	3.95	11.65	0.5	3.57	0	0.17	0	0
48	11.55	11.9	12.45	8.96	9	3.91	0	0.03	0.03
49	22.8	22.3	22.85	6.7	5.4	14.67	15.45	0	0.03
50	1.2	2.25	6.1	1.67	2.23	1.08	2.25	2.07	2.37
51	12.55	13.3	15.7	10.8	10.67	7.79	4.20	1.37	1.7
52	4.85	1.95	9.9	4.27	3.5	0	0.45	0.33	2.07
53	6.1	6.25	16.55	5.53	3.33	0	1.37	3.47	3.83
54	1.35	1	1.7	1.5	1	0.5	0.12	0	0.23
55	10.1	7.65	8.8	11.07	6.27	0	0.17	0	0

56	12.35	13	19.2	1.63	0.23	2.95	14.37	5.4	6.23
57	0.1	0.2	0.35	0.5	0.43	0	0.12	0.07	0.1
58	0.55	1.35	1.6	1.27	0.4	0.20	0.87	0.53	1.13
59	2.65	1.9	2.15	1.1	1.37	1.17	2.41	0.33	0.63
60	4	5.7	30.45	17.47	5.43	0.79	9.41	0.9	2.23
61	4.75	5.25	5.5	5.07	4.6	0.04	0.67	0.03	0.03
62	17.3	15.1	27.45	7.4	1.97	4.12	5	2.7	3.1
63	29.35	29.4	28.9	15.33	18.17	2.17	0	0.63	0.5
64	3.3	1.3	6.1	2.9	2.43	0	0.12	0.03	0.77
65	8	4.75	12.45	2.9	1.9	0	5.67	0	0.03
66	17.25	16	33.75	8.67	16.3	11.54	8.95	4.77	4.3
67	10.65	9.7	12.3	6.97	3.07	9.12	2.29	0	0
68	4.25	3.7	8.1	12.33	2.73	0	1.37	10.67	11.83
69	1.45	3.75	8.85	6.13	1.17	0	2.95	2.9	2.4
70	0	0	0	0.03	0	0	0	0	0
71	0.05	0	0	0.1	0	0	0	0	0
72	0	0	0.35	1.83	0.57	0	0.17	0.57	0.73
73	2.5	2.5	4.55	3.77	0.23	1.04	4.08	0.7	0.87
74	7.9	8.6	9.65	10.27	8.23	0.17	3.83	4.7	5.2
75	3.3	2.1	4.55	0.2	0.6	1.62	1.91	0.47	0.73
76	13.3	17.35	11.1	2.4	13.07	7.79	9.08	0	0.63
77	14.9	14.9	15.45	9.57	10.9	5.58	4.5	0.83	1.26
78	0.9	1.6	1.7	1.23	1.17	0	0	0	0
79	13.9	14.05	17.2	6.8	7.2	6.17	11.79	0	0.07
80	45.85	50.45	51.8	24.9	21.6	17.5	13.58	0.5	1.87
81	7.1	7.65	8.95	2.33	2.07	0.08	0.45	0	0
82	10.25	10.5	10.7	7.73	7.73	3.41	0	0.03	0.4
83	24.2	24.1	23.8	8.6	7.4	18.95	16.41	0.03	0.23
84	3.7	3.45	10.8	2.47	2.97	1.58	2.91	0	1.03
85	13.75	14.1	14.85	10.97	11.27	8.41	3.66	0.4	0.77
86	8.6	8.75	12.35	6.8	5.73	1.83	3.20	0.07	2.43
87	6.85	8.35	11.9	8.47	6.97	0	2.67	3.43	3.7
88	2.5	2.65	3.1	2.03	2	1.5	0.79	0	0
89	6.2	6.35	11.55	9.73	4.73	0	2.83	0	0.7
90	4.2	3.4	6.05	1.9	4.33	2.62	7.95	0.03	1.4
91	0.15	0.15	1.05	0.33	0.43	0.04	0.5	0	0.03
92	0.4	0.2	2.65	0.47	0.93	0.37	1.12	0	0.13
93	3.25	2.25	2.65	1.67	2.47	0.91	4.17	0.56	0.67
94	13.3	9.7	20.9	16.9	5.9	2.7	13.62	2.13	2.6

95	4.15	4.6	5.05	4	3.87	0	0.83	0	0.27
96	9.4	6.5	13.2	5.4	1.67	3.33	6.58	0.87	1.03
97	30.4	31.05	31.3	16.87	19.4	3	0.87	1.23	1.2
98	1.95	1.8	3.15	2.07	1.37	0	0.20	0.03	0.3
99	11.95	10.3	16.25	5.53	5.6	1.33	2.7	0	0.07
100	30.95	23.45	31.2	9.43	10.97	6.83	7.87	2.2	2.17
101	8.25	14.15	15.8	6.03	4.97	9.45	1	0	0
102	9.75	10.35	12.85	14.97	7.23	2.17	1.04	8.87	10.23
103	5.1	9.65	12.9	6.97	2.4	3	2.79	3.37	3.8
104	0.05	0	0.35	0.2	0.1	0	0	0	0
105	0.35	1.8	2.05	0.5	0.2	0.08	0	0	0
106	0	0	0	1.13	0.2	0	1	0.5	0.43
107	4.55	5.1	6.95	4.4	0.8	3.45	5.08	0.07	1

Table A.1: List of the Activated Voxels

Pontifícia Universidade Católica do Rio Grande do Sul
Pró-Reitoria de Graduação
Av. Ipiranga, 6681 - Prédio 1 - 3º. andar
Porto Alegre - RS - Brasil
Fone: (51) 3320-3500 - Fax: (51) 3339-1564
E-mail: prograd@pucrs.br
Site: www.pucrs.br